ADVANCING EARTH AND SPACE SCIENCE

Geophysical Research Letters

RESEARCH LETTER

10.1029/2022GL101185

Key Points:

- Modeling of the Tonga volcanic eruption show equatorial plasma bubbles (EPBs) develop in the Pacific sector
- A large equatorial bubble formed below 500 km roughly 30° in longitude
- EPBs rose to very high altitudes (>4,000 km)

Correspondence to:

J. D. Huba,
jdhuba@syntek.org

Citation:

Huba, J. D., Becker, E., & Vadas, S. L. (2023). Simulation study of the 15 January 2022 Tonga event: Development of super equatorial plasma bubbles. *Geophysical Research Letters*, *50*, e2022GL101185. https://doi.org/10.1029/2022GL101185

Received 8 SEP 2022
Accepted 17 DEC 2022

Simulation Study of the 15 January 2022 Tonga Event: Development of Super Equatorial Plasma Bubbles

J. D. Huba[1], E. Becker[2], and S. L. Vadas[2]

[1]Syntek Technologies, Fairfax, VA, USA, [2]Northwest Research Associates, Boulder, CO, USA

Abstract We present high-resolution simulation results of the response of the ionosphere/plasmasphere system to the 15 January 2022 Tonga volcanic eruption. We use the coupled Sami3 is Also a Model of the Ionosphere ionosphere/plasmasphere model and the HIgh Altitude Mechanistic general Circulation Model whole atmosphere model with primary atmospheric gravity wave effects from the Model for gravity wavE SOurces, Ray trAcing and reConstruction model. We find that the Tonga eruption produced a "super" equatorial plasma bubble (EPB) extending ∼30° in longitude and up to 500 km in altitude with a density depletion of 3 orders of magnitude. We also found a "train" of EPBs developed and extended over the longitude range 150°–200° and that two EPBs reached altitudes over 4,000 km. The primary cause of this behavior is the significant modification of the zonal neutral wind caused by the atmospheric disturbance associated with the eruption, and the subsequent modification of the dynamo electric field.

Plain Language Summary The Hunga Tonga-Hunga Ha'apai volcanic eruption occurred on 15 January 2022 at 04:14 UT and generated a massive atmospheric disturbance that caused major effects in the ionosphere worldwide. Using a high-resolution coupled ionosphere/thermosphere model we show that the changes in the thermospheric winds strongly modified the electrodynamics of the ionosphere. This led to the development of a "train" of equatorial plasma bubbles (EPBs), regions of very low electron density, in the western Pacific sector. Moreover, two EPBs reached unusually high altitudes, over 4,000 km.

1. Introduction

The Hunga Tonga-Hunga Ha'apai volcanic eruption occurred on 15 January 2022 at 04:14 UT. It was estimated to have released ∼9–37 megatons of TNT equivalent (Astafyeva et al., 2022), 61 megatons (Diaz et al., 2022), and up to 200 megatons (Vergoz et al., 2022). The eruption generated a massive atmospheric disturbance that caused major effects on the ionosphere worldwide. Zhang et al. (2022), using total electron content (TEC) data from the Global Navigation Satellite System (GNSS), reported that traveling ionospheric disturbances (TIDs) traveled at ∼300–350 m/s with horizontal wavelengths ∼500–1,000 km, circled the earth three times, and lasted 4 days. Similarly, Themens et al. (2022) reported two large-scale traveling ionospheric disturbances and several medium-scale traveling ionospheric disturbances following the eruption based on GNSS data. Harding et al. (2022) reported extreme fluctuations in the ionospheric wind dynamo based on data from the NASA Ionospheric Connection Explorer (ICON) and Swarm satellites. Le et al. (2022), also using ICON and Swarm data, observed an intensification and directional reversal of the equatorial electrojet caused by strong eastward zonal winds in the *E* region generated by the eruption. Aa et al. (2022) reported a large drop in TEC (∼10 TECU) roughly 45 min after the eruption near the epicenter, and a large plasma depletion along the orbital path of ICON with a radius ∼10°–15°. They reported EPBs across a wide region of Asia-Oceania area with electron density depletions of 2–3 orders of magnitude at 450 km.

In this paper we present high-resolution simulation results of the response of the ionosphere/plasmasphere system to the Tonga volcanic eruption. We use the Sami3 is Also a Model of the Ionosphere (SAMI3) ionosphere/plasmasphere model driven by the neutral winds simulated by the HIgh Altitude Mechanistic general Circulation Model (HIAMCM). The HIAMCM simulates the secondary gravity waves (GWs) and other neutral wind and temperature changes, which were caused by the localized body forces and heatings created from the dissipation of primary GWs from the Tonga eruption computed using the Model for gravity wavE SOurces, Ray trAcing and reConstruction (MESORAC). We simulate the event day 15 January 2022 for two cases: without the Tonga eruption and with the Tonga eruption. By comparing the results of these two cases we can identify the impact of the volcanic eruption on the ionosphere and plasmasphere. We find that the Tonga eruption produced a "super"

EPB extending ∼30° in longitude and up to 500 km in altitude with a density depletion of 3 orders of magnitude, a "train" of EPBs forming over the longitude range 150°–200°, and that two EPBs reached altitudes over 4,000 km. The primary cause of this behavior is the significant modification of the zonal neutral wind caused by the atmospheric disturbance associated with the eruption, and the subsequent modification of the dynamo electric field.

2. Models

SAMI3 is a global model of the ionosphere/plasmasphere system. It is based on the SAMI2 model (Huba et al., 2000). Details on the model have been discussed in previous papers (for e.g., Huba & Joyce, 2010; Huba & Liu, 2020). We note that a feature of the SAMI3 model used in this study is the implementation of a fourth order flux-corrected transport scheme for $\mathbf{E} \times \mathbf{B}$ transport perpendicular to the magnetic field. The partial donor cell method (Hain, 1987; J. D. Huba, 2003) is used which reduces numerical diffusion and allows steep density gradients to develop on the sides of equatorial plasma bubbles (EPBs).

The HIAMCM is a high-resolution whole-atmosphere model for the neutral dynamics that simulates GWs explicitly from the surface to the thermosphere. The effective resolution corresponds to horizontal and vertical wavelengths of about 200 and 2 km, respectively. In the present study, the large scales of the model are nudged to MERRA-2 reanalysis in the troposphere and stratosphere, thereby allowing for the simulation of observed events. The GWs simulated by the nudged HIAMCM have been shown to agree with observations (Becker & Vadas, 2020; Becker et al., 2021, 2022). The current setup of the HIAMCM is for solar minimum conditions and the highest model layer is at $z \sim 400$ km.

Since even the high-resolution HIAMCM cannot resolve the primary GWs excited by the strong updrafts of air generated by the Tonga eruption, we use GOES satellite data and the MESORAC model to provide the perturbations to the HIAMCM. To this end, we determined the parameters of the updrafts from GOES-17 cloud top temperatures and computed the spectrum of primary GWs excited by the volcanic eruption (S. L. Vadas, 2013; Vadas & Fritts, 2009; Vadas et al., 2009, 2012). We ray-traced these primary GWs into the mesosphere and thermosphere using the model of Vadas and Fritts (2009). The background atmosphere for the ray tracing was the large-scale flow from the HIAMCM simulation without the perturbations from MESORAC. When the ray-traced GWs dissipated from saturation and/or molecular diffusion, they generated highly localized and intermittent body forces and heatings. These ambient-flow effects were computed after reconstructing the primary GW field (including positive and negative interference) as described in S. L. Vadas (2013). We found that the majority of the ambient-flow effects typically occurred in the mesosphere and thermosphere up to about 200–250 km in the vicinity of the volcano, that is from about 180°E to 190° E and 30°S to 10° S. These effects were largest 50–70 min after the first eruption. These body forces and heatings were then implemented into the HIAMCM, and the HIAMCM simulation was repeated starting at 3 UT on 15 January (2022). The HIAMCM with the perturbation from the Tonga eruption yields the secondary GWs triggered by the event. We find that the secondary GWs simulated by the HIAMCM have horizontal phase speeds of 100-750 m/s and horizontal wavelengths of 400–7,500 km, which agree well with the GWs observed by ICON. This is in contrast to the Lamb waves excited by Tonga, which only have horizontal phase speeds of 300–320 m/s and horizontal wavelengths of 100–200 km (Wright et al., 2022).

Other simulation parameters are as follows. The horizontal grid for post-processed HIAMCM output is 0.5° × 0.5° in latitude and longitude, and covers the entire earth. The SAMI3 grid is also 0.5° in longitude but is variable in latitude. The grid in latitude is ∼1° for latitudes around 40°, decreases to ∼0.15° near the magnetic equator, and increases to ∼1.5° in the high-latitude region. The SAMI3 grid in magnetic latitude is ±89°.

Two simulations are considered. The first simulation is for 15 January 2022 without the Tonga atmospheric disturbance while the second simulation is for 15 January 2022 with the Tonga disturbance. This allows us to assess the direct impact of the Tonga event on the ionosphere/thermosphere system by comparing the results from the two simulations. The solar activity indices used are F10.7 = 111 and F10.7A= 111, and with Ap = 20. We point out that this day was in the recovery stage of a medium geomagnetic storm (Dst ∼ −90 on 14 January 2022 at 22:00 UT) and that the impact of the storm on the ionosphere/thermosphere system is not considered in the current study. However, Le et al. (2022) reported that the storm had minimal impact on the equatorial electric field.

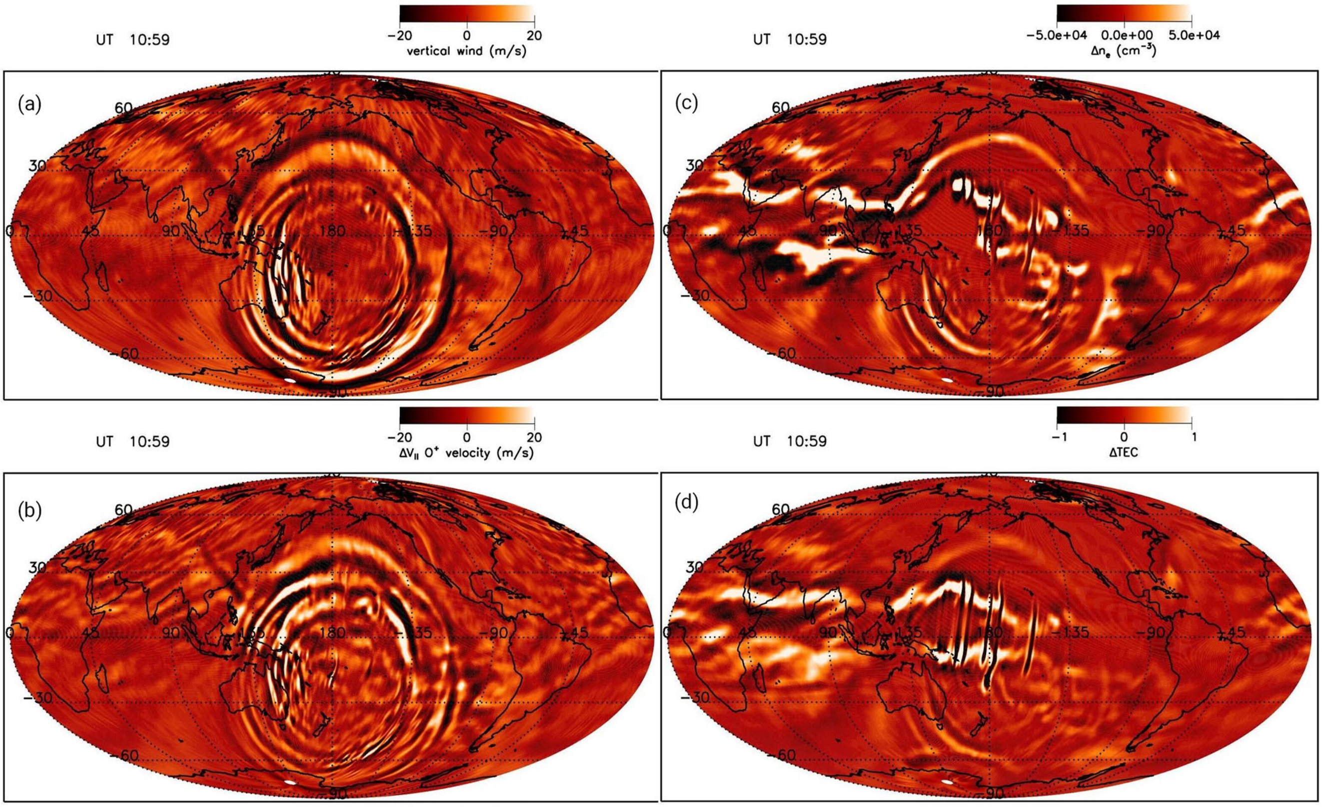

Figure 1. Contour plots of the (a) vertical neutral wind, (b) the perturbed O^+ velocity parallel to the magnetic field, (c) the perturbed electron density at an altitude 293 km, and (d) the perturbed total electron content at time 10:59 UT for the "Tonga" case.

3. Results

In Figure 1 we show contour plots of (a) the vertical neutral wind, (b) the perturbed O^+ velocity parallel to the magnetic field, (c) the perturbed electron density at an altitude 293 km, and (d) the perturbed TEC at time 12:59 UT for the "Tonga" case. Here, the perturbed O^+ parallel velocity, electron density, and TEC are $\Delta V_\parallel = V_\parallel - V_{\parallel s}$, $\Delta n_e = n_e - n_{es}$, $\Delta\text{TEC} = \text{TEC} - \text{TEC}_s$, respectively, where the subscript "s" denotes a smoothed profile. Here the smoothed profile was obtained using the Interactive Data Language smooth function with an input parameter 2. In Figure 1a we see the clear impact of the Tonga disturbance on the vertical neutral wind: concentric rings of neutral wind fluctuations emanating from the location of the volcanic eruption (20°S latitude and 175°W longitude). In Figure 1b there is also a concentric ring of O^+ parallel velocity variations that roughly coincide with the neutral wind variations in Figure 1a, since the perturbed vertical wind can move the plasma along the magnetic field line because of collisional coupling. We note that the parallel O^+ velocity is positive in the northward direction. Thus, in the southern hemisphere the vertical wind and O^+ velocity will be "in phase" while in the northern hemisphere they will be "out of phase." A similar concentric pattern of oscillations also occurs for the perturbed electron density seen in Figure 1c. More interesting is the appearance of the elongated structures in the equatorial region in Figure 1c which are associated with the development of EPBs. This more clearly illustrated in Figure 1d which shows ΔTEC. Several elongated striations are evident in the center of the figure which are EPBs, one of which extends ∼±30° in latitude. We note that Rajesh et al. (2022) reported EPBs reaching ∼40°N in the longitude range 100°–150° based on the rate of total electron content index.

In Figure 2 we present contour plots of the zonal neutral wind as a function of longitude and altitude in the magnetic equatorial plane for the "no Tonga" case (a, b) and the "Tonga" case (c, d) at times 07:59 UT (a, c) and 10:59 UT (b, d). Red denotes an eastward zonal wind and blue denotes a westward neutral wind. At time 07:59 UT, there is a predominant eastward drift in the "no Tonga" case (a) for longitudes >160°; this is in the early evening local time. However, for the "Tonga" case (c) the zonal wind is significantly modified: there are strong reversals of the wind with westward drifts at longitudes ∼145°, 160°, and 205°. At time 10:59 UT there are

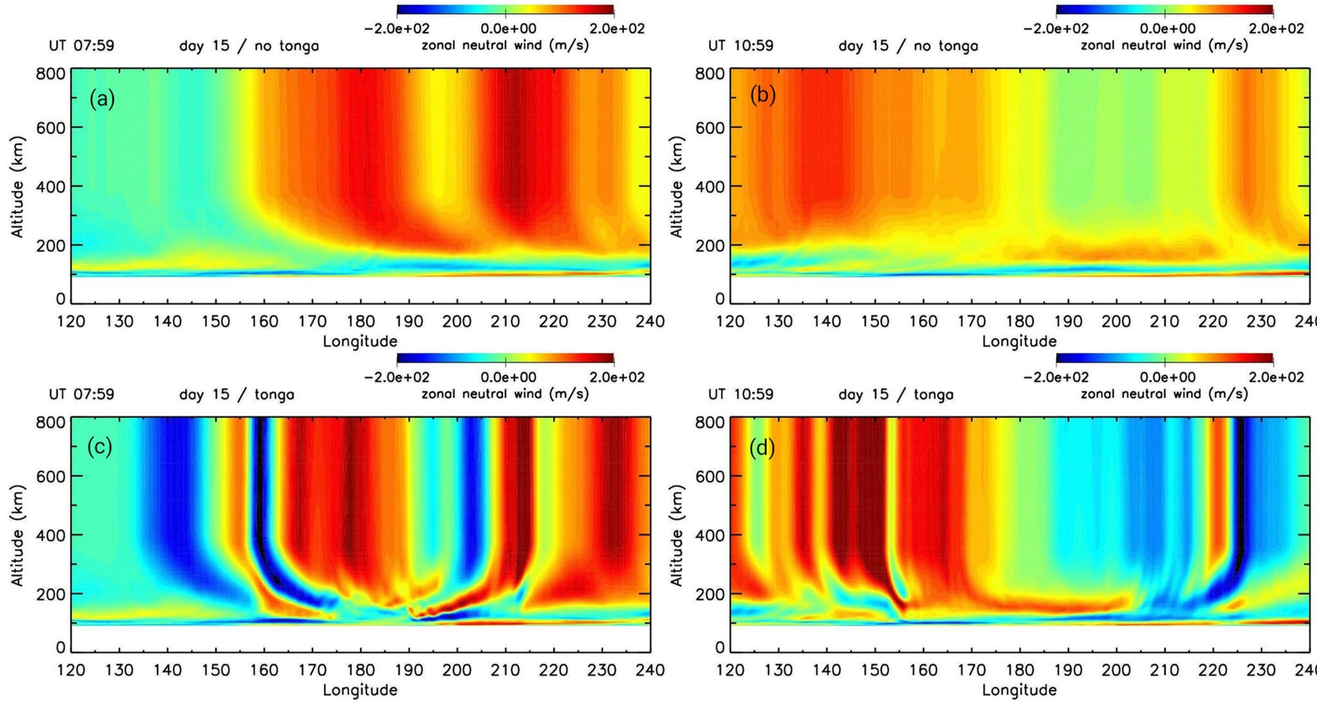

Figure 2. Contour plots of the zonal neutral wind as a function of longitude and altitude in the magnetic equatorial plane for the "no Tonga" case (a and b) and the "Tonga" case (c and d) at times 07:59 UT (a and c) and 10:59 UT (b and d).

eastward drifts in the F region for both the "no Tonga" and "Tonga" cases in the longitude range 120°–180°; however, the "Tonga" case has stronger and more structured drifts. Additionally, there are regions of westward drifts for the "Tonga" case for longitudes >190° that are absent in the "no Tonga" case.

In Figure 3 we show contour plots of the vertical $E \times B$ velocity as a function of longitude and altitude in the magnetic equatorial plane for the "no Tonga" case (a, b) and the "Tonga" case (c, d) at times 07:59 UT (a, c) and 10:59 UT (b, d). There are significant differences between the "no Tonga" case and "Tonga" case; this is to be expected because the vertical $E \times B$ plasma drift is largely controlled by the zonal neutral wind in the low-latitude ionosphere and there are large differences in the zonal wind for the two cases as shown in Figure 2. At time 07:59 UT for the "no Tonga" case (a) there is an upward drift of $\lesssim$30 m/s in the longitude range 150°–180° which corresponds to local times 18:00 LT–20:00 LT; this is associated with the pre-reversal enhancement of the eastward electric field. On the other hand, for the "Tonga" case (c), the upward drift is larger and spans a broader longitude range albeit not uniform. At time 10:59 UT there are two channels of large upward drifts for the "no Tonga" case (b); these are associated with the development of two EPBs. For the "Tonga" case (d) there several upward channels extending from 150° to 230°. Of note is the large upward drift in the range 150°–160° extending from less than 200 km to over 800 km. Additionally there are regions of strong downward drifts.

In Figure 4 we show contour plots of the electron density as a function of longitude and altitude in the magnetic equatorial plane for the "no Tonga" case (a, b, e, f) and the "Tonga" case (c, d, g, h) at times 07:59 UT (a, c), 10:59 UT (b, d), 12:59 UT (e, g), and 19:59 UT (f, h). At time 07:59 UT, differences between the "no Tonga" case (a) and "Tonga" case (c) begin to appear at the magnetic equator. There is an uplift in the bottomside F region ionosphere for the "Tonga" case relative to the "no Tonga" case at longitudes ~167° and 190° associated with the enhanced upward velocities at this time. At time 10:59 UT the differences are more dramatic. Two EPBs have formed and penetrated the topside of the F region for the "no Tonga" case (b). However, for the "Tonga" case (d) the F region is substantially modified. First, there are six EPBs that formed and have penetrated into the topside, and three are higher than 800 km. Second, there is a very large depletion in the electron density above 400 km in the longitude range ~150°–170°. This spans a range of ~2,300 km in the zonal direction. And lastly, aside from an uplift of the ionosphere and the development of EPBs, there are also several regions where the ionosphere descends relative to the "no Tonga" case. Specifically, there are enhancements of the electron density

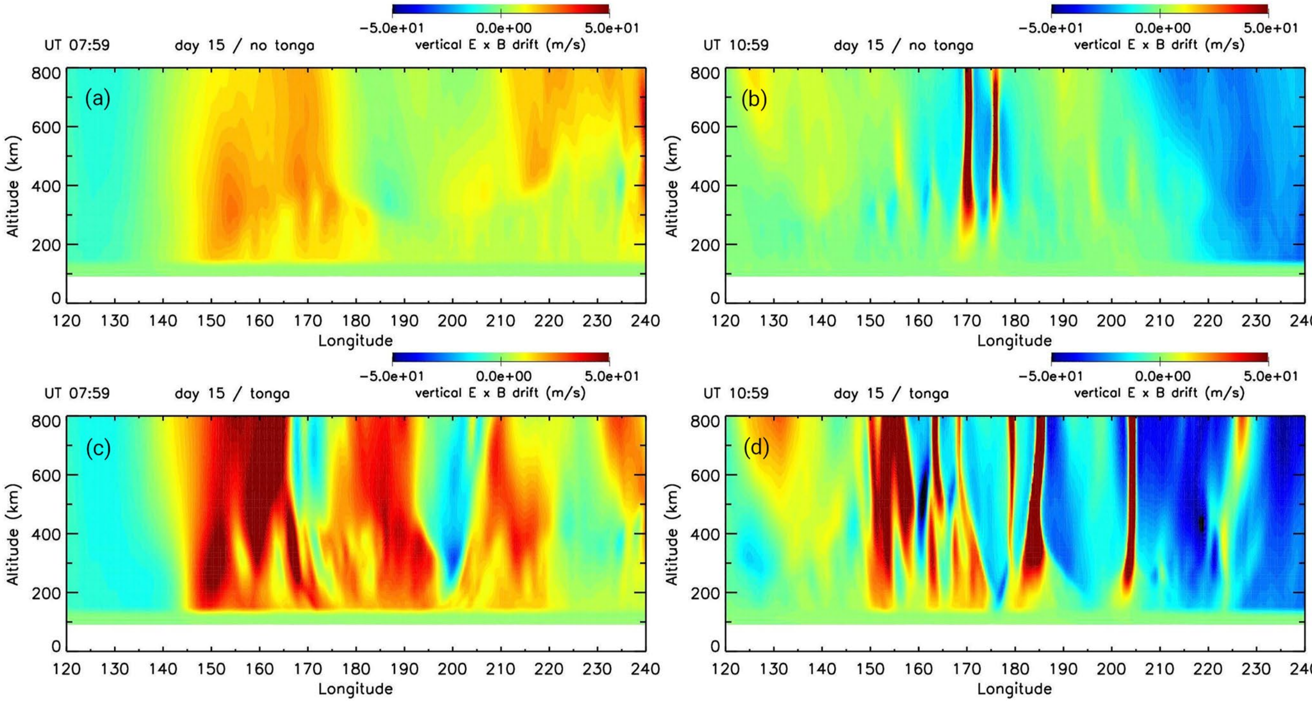

Figure 3. Contour plots of the vertical $E \times B$ velocity as a function of longitude and altitude in the magnetic equatorial plane for the "no Tonga" case (a and b) and the "Tonga" case (c and d) at times 07:59 UT (a and c) and 10:59 UT (b and d).

below ~300 km in the longitude range ~176° and 195° associated with the downward flows in these regions (see Figure 3d).

In Figures 4e–4h the altitude range is increased to 4,800 km from 800 km. In Figure 4e (the "no Tonga event" case) the two EPBs that had developed in Figure 4b have penetrated the *F* layer at ~172° and ~177° but do not lead to large plasma depletions on the topside. On the other hand, two of the EPBs generated during "the Tonga event" have risen to over 2,000 km and exhibit deep depletions in Figure 4g. These depletions drift eastward (Figure 4h) and eventually reach altitudes ~4,000 km at 19:29 UT and remain relatively "deep" (i.e., a factor of 5 decrease in electron density from the surrounding environment). The upward velocity of these EPBs is ~200 m/s Rajesh et al. (2022) reported EPBs rising at a rapid velocity (e.g., ~280–420 m/s) up to 1,500 km and then slowing to ~200 m/s consistent with our results, albeit at different longitudes. They also show disturbances in the altitude range 1,000–3,000 km around longitude 150° at time 11:50 UT. In Figure 4g an EPB reaches ~2,400 km at 155° at 12:29 UT; somewhat later than in the observations but qualitatively consistent. Additionally, there is an impact of the "Tonga" event on the inner plasmasphere evidenced by the reduced electron density in the range ~150°–180° at 4,800 km altitude.

In Figure 5 we show plots of the electron density (a, b) and vertical $E \times B$ drift (c, d) as a function of longitude at altitudes 488 km (a, c) and 607 km (b, d) at time 10:59 UT in the magnetic equatorial plane for the "Tonga" case. At 488 km a large EPB has developed in the range 140°–170° (a) with a very deep depletion of ~3 orders of magnitude. Over this range the $E \times B$ drift is upwards with a maximum velocity ~70 m/s (c). A very deep, narrow EPB has formed at 185° and a smaller, narrow depletion at 205°, both with upward drifts exceeding 200 m/s. At the higher altitude 607 km, the broad depletion has developed into 3 narrower depletions (b) with somewhat larger upward $E \times B$ drifts (d) than at the lower altitude.

These results for 607 km in Figures 5b and 5d are at an altitude similar to that of the ICON satellite (but are not in ICON path). Nonetheless we can roughly compare these results to similar results presented in Aa et al. (2022) based on ICON-Ion Velocity Meter (IVM) measurements. Aa et al. (2022) show numerous EPBs observed by ICON-IVM in the range 150°–200° that begin at ~07:00 UT and persist to at least 12:19 UT. The EPBs shown in Figure 5b resemble those observed by ICON-IVM at these times. However, at times 07:52 UT–08:51 UT there are also observations of several EPBs with upward drifts of ~100 m/s in this range; this is in contrast

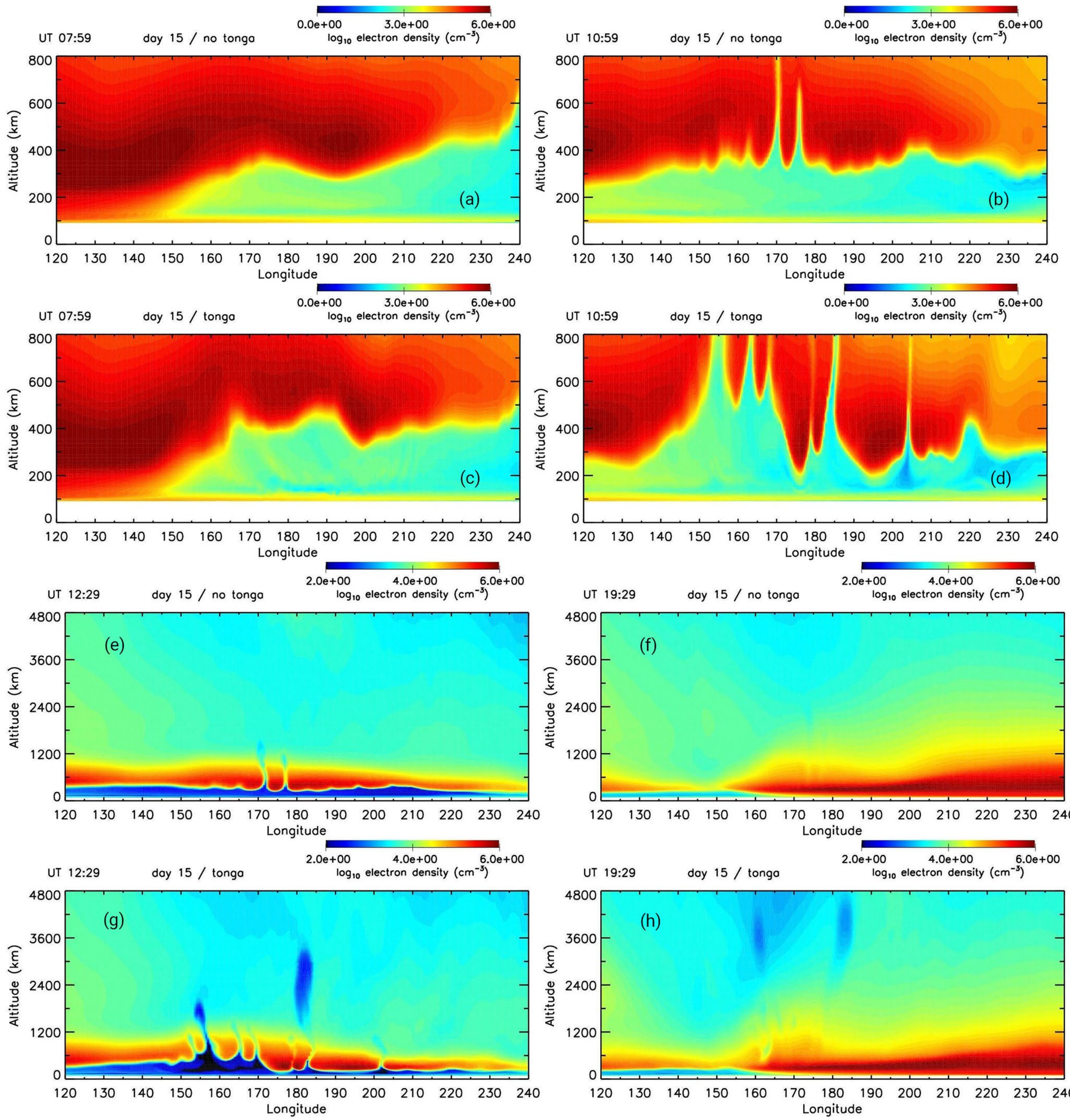

Figure 4. Contour plots of the electron density as a function of longitude and altitude in the magnetic equatorial plane for the "no Tonga" case (a and b) and the "Tonga" case (c and d) at times 07:59 UT (a and c) and 10:59 UT (b and d), and the "no Tonga" case (e and f) and the "Tonga" case (g and h) at times 12:59 UT (e and g) and 19:59 UT (f and h).

to the electron density in Figure 4c which does not show any EPBs at 7:59 UT. However, the zonal variations of the upward drifts in Figure 5c are similar to those in reported in Aa et al. (2022), albeit smaller. Moreover, Aa et al. (2022) reported electron density depletions of 3 orders of magnitude (down to $n_e \sim 10^3$ cm^{-3}) similar to our results.

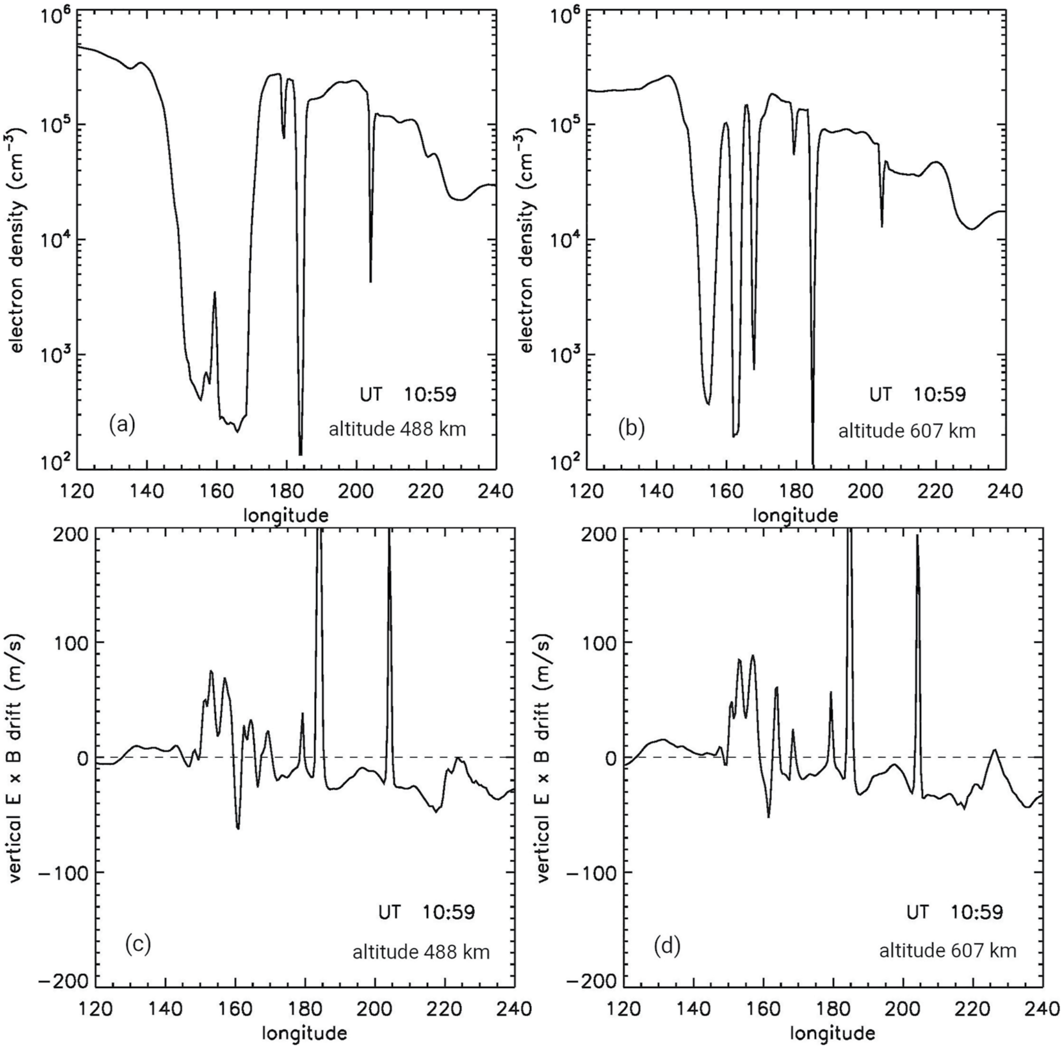

Figure 5. Plots of the electron density (a and b) and vertical $E \times B$ drift (c and d) as a function of longitude at altitudes 488 km (a and c) and 607 km (b and d) at time 10:59 UT in the magnetic equatorial plane for the "Tonga" case.

4. Summary

In this paper we present high-resolution simulation results of the response of the ionosphere/plasmasphere system to the Tonga volcanic eruption using the coupled SAMI3 ionosphere/plasmasphere model and the HIAMCM whole atmosphere model with added primary GW effects from the MESORAC model. We simulated the event day 15 January 2022 for two cases: without the Tonga eruption and with the Tonga eruption. By comparing the results of these two cases we can identify the impact of the volcanic eruption on the ionosphere and plasmasphere. We find that the Tonga eruption produced a "super" EPB extending ∼30° in longitude up to 500 km with a density depletion of 3 orders of magnitude centered around 160° longitude. This was caused by an upward plasma drift transporting low density plasma in the bottomside *F* region to higher altitudes. We also found a "train" of EPBs formed over the longitude range 150°–200°, mostly west of the eruption's epicenter. Lastly, two EPBs reached very high altitudes, over 4,000 km, which is significantly higher than observed in previous simulation studies (for e.g., Huba & Liu, 2020).

Aa et al. (2022) reported a broad density depletion developed at the ICON altitude (∼600 km) centered around the Tonga epicenter longitude 185°. In contrast we find a narrow EPB formed (see Figure 5c). Additionally, a series of EPBs was shown to develop in Aa et al. (2022) that drifted westward to ∼120°; the EPBs that developed in our simulation study did not exhibit a westward drift. Also, the EPBs reported in Aa et al. (2022) formed about an hour earlier than the ones in our simulation study. The simulation results qualitatively captured the results reported in Aa et al. (2022) but better quantitative agreement requires further study and simulations.

Data Availability Statement

Data used in this paper is available at https://doi.org/10.5281/zenodo.7051074.

Acknowledgments
This research was supported by NASA Grants NNH17ZDA001N07 and NNG12FA45C, AFOSR Grant F4FGA01252A005, and NSF Grant AGS-1931415 [JDH], and NASA Grant 80NSSC19K0836 [EB,SV], and NASA Grant 80NSSC22K0174 [JDH,EB,SV].

References

Aa, E., Zhang, S.-R., Erickson, P. J., Vierinen, J., Coster, A. J., Goncharenko, L. P., et al. (2022). Significant ionospheric hole and equatorial plasma bubbles after the 2022 Tonga volcano eruption. *Space Weather*, *20*(7), e2022SW003101. https://doi.org/10.1029/2022SW003101

Astafyeva, E., Maletckii, B., Mikesell, T. D., Munaibari, E., Ravanelli, M., Coisson, P., et al. (2022). The 15 January 2022 Hunga Tonga eruption history as inferred from ionospheric observations. *Geophysical Research Letters*, *49*(10), e2022GL098827. https://doi.org/10.1029/2022GL098827

Becker, E., Goncharenko, L., Harvey, V. L., & Vadas, S. L. (2022). Multi-step vertical coupling during the January 2017 sudden stratospheric warming. *Journal of Geophysical Research*, *127*, e2022JA030866. https://doi.org/10.1029/2022JA030866

Becker, E., & Vadas, S. L. (2020). Explicit global simulation of gravity waves in the thermosphere. *Journal of Geophysical Research: Space Physics*, *125*(10), e2020JA028034. https://doi.org/10.1029/2020JA028034

Becker, E., Vadas, S. L., Bossert, K., Harvey, V. L., Zülicke, C., & Hoffman, L. (2021). A High-resolution whole-atmosphere model with resolved gravity waves and specified large-scale dynamics in the troposphere and stratosphere. *Journal of Geophysical Research: Atmospheres*, *127*(2), e2021JD035018. https://doi.org/10.1029/2021JD035018

Díaz, J. S., & Rigby, S. E. (2022). Energetic output of the 2022 Hunga Tonga–Hunga Ha'apai volcanic eruption from pressure measurements. *Shock Waves*, *32*(6), 553–561. https://doi.org/10.1007/s00193-022-01092-4

Hain, K. (1987). The partial donor cell method. *Journal of Computational Physics*, *73*(1), 131–147. https://doi.org/10.1016/0021-9991(87)90110-0

Harding, B. J., Wu, Y.-J. J., Alken, P., Yamazaki, Y., Triplett, C. C., Immel, T. J., et al. (2022). Impacts of the January 2022 Tonga volcanic eruption on the ionospheric dynamo: ICON-MIGHTI and Swarm observations of extreme neutral winds and currents. *Geophysical Research Letters*, *49*(9), e2022GL098577. https://doi.org/10.1029/2022GL098577

Huba, J. D. (2003). A tutorial on Hall magnetohydrodynamics. In M. Scholer, C. T. Dum, & J. Büchner (Eds.), *Space simulations*. Springer. 170.

Huba, J. D., & Joyce, G. (2010). Global modeling of equatorial plasma bubbles. *Geophysical Research Letters*, *37*(17), L17104. https://doi.org/10.1029/2010GL044281

Huba, J. D., Joyce, G., & Fedder, J. A. (2000). SAMI2 (Sami2 is another model of the ionosphere): A new low-latitude ionosphere model. *Journal of Geophysical Research*, *105*(A10), 23035–23053. https://doi.org/10.1029/2000ja000035

Huba, J. D., & Liu, H.-L. (2020). Global modeling of equatorial spread *F* with SAMI3/WACCM-X. *Geophysical Research Letters*, *47*(14), e2020GL088258. https://doi.org/10.1029/2020GL088258

Le, G., Liu, G., Yizengaw, E., & Englert, C. R. (2022). Intense equatorial electrojet and counter electrojet caused by the 15 January 2022 Tonga volcanic eruption: Space- and ground-based observations. *Geophysical Research Letters*, *49*(11), e2022GL099002. https://doi.org/10.1029/2022GL099002

Rajesh, P. K., Lin, C. C. H., Lin, J. T., Lin, C. Y., Liu, J. Y., Matsuo, T., et al. (2022). Extreme poleward expanding super plasma bubbles over Asia-Pacific region triggered by Tonga volcano eruption during the recovery-phase of geomagnetic storm. *Geophysical Research Letters*, *49*(15), e2022GL099798. https://doi.org/10.1029/2022GL099798

Themens, D. R., Watson, C., ÂŽagar, N., Vasylkevych, S., Elvidge, S., McCaffrey, A., et al. (2022). Global propagation of ionospheric disturbances associated with the 2022 Tonga volcanic eruption. *Geophysical Research Letters*, *49*, e2022GL098158. https://doi.org/10.1029/2022GL098158

Vadas, S. L. (2013). Compressible f-plane solutions to body forces, heatings, and coolings, and application to the primary and secondary gravity waves generated by a deep convective plume. *Journal of Geophysical Research*, *118*(5), 2377–2397. https://doi.org/10.1002/jgra.50163

Vadas, S. L., & Fritts, D. C. (2009). Reconstruction of the gravity wave field from convective plumes via ray tracing. *Annales geophysicae*, *27*(1), 147–177. https://doi.org/10.5194/angeo-27-147-2009

Vadas, S. L., Yue, J., & Nakamura, T. (2012). Mesospheric concentric gravity waves generated by multiple convection storms over the North America great plain. *Journal of Geophysical Research*, *117*, D7. https://doi.org/10.1029/2011JD017025

Vadas, S. L., Yue, J., She, J., Stamus, P., & Liu, A. (2009). A model study of the effects of winds on concentric rings of gravity waves from a convective plume near Fort Collins on 11 May 2004. *Journal of Geophysical Research*, *114*(D6), D06103. https://doi.org/10.1029/2008JD010753

Vergoz, J., Hupe, P., Listowski, C., Le Pichon, A., Garcés, M. A., Marchetti, E., et al. (2022). IMS observations of infrasound and acoustic-gravity waves produced by the January 2022 volcanic eruption of Hunga, Tonga: A global analysis. *Earth and Planetary Science Letters*, *591*, 117639. https://doi.org/10.1016/j.epsl.2022.117639

Wright, C., Hindley, N., Alexander, M. J., Barlow, M., Hoffmann, L., Mitchell, C., et al. (2022). Surface-to-space atmospheric waves from Hunga Tonga-Hunga Hápai eruption. *Earth and Space Science Open Archive*, *23*, 2269. https://doi.org/10.1002/essoar.10510674.2

Zhang, S.-R., Vierinen, J., Aa, E., Goncharenko, L. P., Erickson, P. J., Rideout, W., et al. (2022). Tonga volcanic eruption induced global propagation of ionospheric disturbances via Lamb waves. *Frontiers in Astron. Space Science*, *15*. https://doi.org/10.3389/fspas.2022.871275